State of Charge Estimation for Lithium-ion Batteries:An Adaptive Approach

Fang, H.; Wang, Y.; Sahinoglu, Z.; Wada, T.; Hara, S.

Abstract

State of charge (SoC) estimation is of key importance in the design of battery management systems. An adaptive SoC estimator, which is named AdaptSoC, is developed in this paper. It is able to estimate the SoC in real time when the model parameters are unknown, via joint state (SoC) and parameter estimation. The AdaptSoC algorithm is designed on the basis of three procedures. First, a reduced-complexity battery model in state-space form is developed from the well-known single particle model (SPM). Then a joint local observability/identifiability analysis of the SoC and the unknown model parameters is performed. Finally, the SoC is estimated simultaneously with the parameters using the iterated extended Kalman filter (IEKF). Simulation and experimental results exhibit the effectiveness of the AdaptSoC.

State of Charge Estimation for Lithium-ion Batteries: An Adaptive Approach

Huazhen Fang[a], Yebin Wang[b,1], Zafer Sahinoglu[b], Toshihiro Wada[c], Satoshi Hara[c]

[a]*Department of Mechanical & Aerospace Engineering, University of California, San Diego, CA 92093, USA*
[b]*Mitsubishi Electric Research Laboratories, 201 Broadway, Cambridge, MA 02139, USA*
[c]*Advanced Technology R&D Center, Mitsubishi Electric Corporation, 8-1-1, Tsukaguchi-honmachi, Amagasaki City, 661-8661, Japan*

Abstract

State of charge (SoC) estimation is of key importance in the design of battery management systems. An adaptive SoC estimator, which is named `AdaptSoC`, is developed in this paper. It is able to estimate the SoC in real time when the model parameters are unknown, via joint state (SoC) and parameter estimation. The `AdaptSoC` algorithm is designed on the basis of three procedures. First, a reduced-complexity battery model in state-space form is developed from the well-known single particle model (SPM). Then a joint local observability/identifiability analysis of the SoC and the unknown model parameters is performed. Finally, the SoC is estimated simultaneously with the parameters using the iterated extended Kalman filter (IEKF). Simulation and experimental results exhibit the effectiveness of the `AdaptSoC`.

Keywords: State of charge, Li$^+$ battery, state and parameter estimation, adaptive estimation, iterated extended Kalman filter

1. Introduction

Lithium-ion (Li$^+$) batteries have gained widespread use in numerous applications from consumer electronics to power tools soon after their first commercialization in 1991, thanks to their higher capacity but reduced size, superior power performance with longer cycle life [1]. Recent advances in electric vehicles and smart grids further strengthen the leading role of Li$^+$ batteries as electrical energy storage devices. Nowadays battery management systems (BMSs) are used in almost all Li$^+$ battery powered applications to monitor the

---

[1]Corresponding author. Tel: 001-617-621-7500; fax: 001-617-621-7550. Email address: yebin-wang@ieee.org

battery status and regulate the charging and discharging processes for real-time battery protection and performance enhancement [2, 3]. A fundamental component in a BMS is the module for estimation of the state of charge (SoC), the design of which has been a long-standing challenge and will be the focus of this paper.

Literature review: SoC can be defined as the percentage ratio of the present battery capacity to the maximum capacity. Two straightforward yet typical *non-model-based* SoC estimation methods are voltage translation and Coulomb counting. The former infers the SoC from the predetermined open circuit voltage (OCV)-SoC lookup table using the OCV measurement. Despite reliability, it requires the battery to rest for a long period with cutting off from the external circuit to measure the OCV, thus restricting its practical implementation without interrupting system operation. Coulomb counting, which is based on numerical integration of the current over time, may suffer from a 'drift' of SoC estimates from the true values due to cumulative integration errors and noise corruption. For a survey of both methods, please refer to [3, 4] and the references therein.

In recent years, considerable attention has been directed toward *model-based* approaches for real-time SoC estimation with improved accuracy. Equivalent circuit models (ECMs), which include virtual voltage source, internal resistance and RC network to simulate battery dynamics, have been used extensively. The state observability of a ECM is studied in [5], by which a SoC estimation algorithm is designed. In [6], the extended Kalman filter (EKF) is applied to ECMs to estimate the SoC with approximate dynamic error bounds. The estimation results are enhanced in [7] using the sigma-point Kalman Filter (SPKF) that is known to have better accuracy and numerical stability. Other nonlinear observer-based design approaches have also been used to construct ECM based SoC estimators. Among them, sliding mode observer [8], adaptive model reference observer [9] and Lyapunov-based observer [10] are highlighted here.

Another important type of battery models are built upon electrochemical principles that describe intercalation and deintercalation of Li$^+$ ions and conservation of charge within a battery. Such electrochemical models have the merit of ensuring each model parameter to retain a proper physical meaning. However, they have a complex structure based on partial differential equations (PDEs), often necessitating model simplification or reduction. A linear reduced-order electrochemical model is established in [11], to which the classical KF is employed for SoC estimation. In [12], the EKF is implemented to estimate SoC using an ordinary differential equation (ODE) model obtained from PDEs by finite-difference discretization. The unscented Kalman filter (UKF) is used in [13] to avoid model linearization

2

in SoC estimation. Rather than using the ODE model after simplification, nonlinear SoC estimators are also developed in [14, 15] through direct manipulation of PDEs.

Adaptive SoC estimation, which enables the SoC to be estimated when the model parameters are unavailable, has been discussed for some ECMs and electrochemical models, e.g., [7, 16, 17]. This paper makes new contributions to study of this topic, with the aim of developing an adaptive SoC estimator that is easy to implement and sound both theoretically and practically.

Statement of contributions: An electrochemical battery model with reduced complexity in structure is derived from the single particle model (SPM) first. For this model, a detailed analysis of joint local observability/identifiability of the SoC variable and the model parameters is performed, which indicates that the SoC variable can be locally identified for admissible input. This result shows that adaptive estimation of SoC is achievable. On the basis of the analysis, an adaptive SoC estimator, `AdaptSoC`, is built using the iterated extended Kalman filter (IEKF), where the SoC and model parameters are estimated concurrently but only SoC estimates are reliable. Through both simulation and experimental study, the `AdaptSoC` algorithm is shown to have excellent SoC estimation performance in the presence of unknown parameters. Meanwhile, its efficient implementation lends itself to practical application. The analysis and results presented in this paper can also be readily extended to other types of battery models.

2. A Reduced-Complexity Model

In this section, the working mechanism of Li^+ batteries is briefly introduced first, followed by a review of the single particle model (SPM). Then a reduction of the SPM is developed for the purpose of SoC estimation.

2.1. The Working Mechanism of Li^+ Batteries

A schematic description of a Li^+ battery is shown in Fig 1(a). The positive electrode is typically made from Li compounds, e.g., $Li_xMn_2O_4$ and Li_xCoO_2. Small solid particles of the compounds are compressed together, giving birth to a porous structure. The negative electrode is also porous, which usually contains graphite particles. The interstitial pores at both electrodes provide intercalation space, where the Li^+ ions can be moved in and out and stored. The electrolyte contains free ions and is electrically conductive, where the Li^+ ions can be transported easily. The separator physically separates the electrodes apart. It allows

3
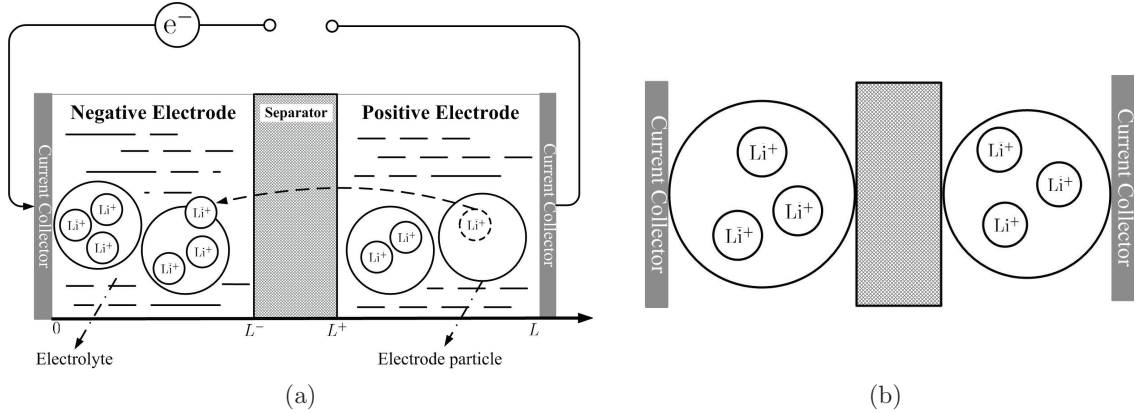
Figure 1: (a) Schematic characterization of a Li$^+$ battery; (b) the single-particle model.

the migration of Li$^+$ ions from one side to the other, but prevents electrons from passing through. The electrons are thus forced to flow through the external circuit.

During the charging process, Li$^+$ ions are extracted from the particles at the positive electrode into the electrolyte, and the particles at the negative electrode absorbs Li$^+$ ions from the electrolyte. This process not only generates an influx of Li$^+$ ions within the battery, but also builds up a potential difference between the positive and negative electrodes. In the reverse process the battery becomes discharged. The following equations exemplify the chemical reactions in the positive and negative electrodes:

$$\mathrm{Li}_x\mathrm{Mn}_2\mathrm{O}_4 \underset{\text{discharge}}{\overset{\text{charge}}{\rightleftharpoons}} \mathrm{Li}_{x-y}\mathrm{Mn}_2\mathrm{O}_4 + y\,\mathrm{Li}^+ + y\,\mathrm{e}^-$$

$$x\,\mathrm{Li}^+ + x\,\mathrm{e}^- + \mathrm{C} \underset{\text{discharge}}{\overset{\text{charge}}{\rightleftharpoons}} \mathrm{Li}_x\mathrm{C}$$
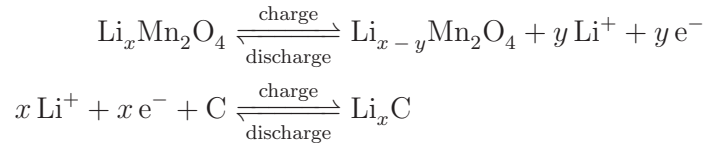
2.2. The Single Particle Model

This paper considers the SPM (see Fig. 1(b)), which, as the name suggests, simplifies each electrode as a spherical particle with area equivalent to the active area of this electrode [18, 19]. Although only able to capture key physical and chemical phenomena, it decreases complexities in identification, estimation and control design for battery operations to a large extent [12, 15]. To proceed further, an introduction of the SPM is given below, with the nomenclature shown in Table 1.

Input and output of the battery: The external input to the battery is the current $I(t)$ with $I(t) < 0$ for charge and $I(t) > 0$ for discharge. The output terminal voltage is the potential difference between the two electrodes, that is,

$$V(t) = \Phi_{s,p}(t) - \Phi_{s,n}(t). \tag{1}$$

4

Variables

Φ_s	electric potential in the solid electrode
Φ_e	electric potential in the electrolyte
c_s	concentration of Li$^+$ in the solid electrode
c_{ss}	concentration of Li$^+$ at a particle's spherical surface
J	molar flux of Li$^+$ at the particle's surface
J_0	exchange current density
η	overpotential of reaction in the cell
U	open-circuit potential
I	external circuit current
V	terminal voltage
r	radial dimension of the particle

Physical parameters

D_s	diffusion coefficient of Li$^+$ in the solid electrode
$\bar{r}$	radius of the spherical particle
F	Farady's constant
S	specific interfacial area
T	temperature of the cell
α^a	anodic charge transport coefficient
α^c	cathodic charge transport coefficient
R	universal gas constant
R_c	phase resistance
R_f	film resistance of the solid electrolyte interphase
ρ	Coulombic efficiency of the cell
C_n	nominal capacity of the cell

Subscripts

s	solid electrode phase
e	electrolyte phase
n	negative electrode
p	positive electrode
j	n or p

Table 1: Definitions and nomenclature.

Conservation of Li$^+$ in the electrode phase: The migration of Li$^+$ ions inside a solid particle is caused by the gradient-induced diffusion. It follows from the Fick's laws of diffusion that

$$\frac{\partial c_{s,j}(r,t)}{\partial t} = \frac{1}{r^2}\frac{\partial}{\partial r}\left(D_{s,j}r^2\frac{\partial c_{s,j}(r,t)}{\partial r}\right), \tag{2}$$

with the initial and boundary conditions given by

$$c_{s,j}(r,0) = c_s^0, \quad \left.\frac{\partial c_{s,j}}{\partial r}\right|_{r=0} = 0, \quad \left.\frac{\partial c_{s,j}}{\partial r}\right|_{r=\bar{r}_j} = -\frac{1}{D_{s,j}}J_j.$$

Here, J_j is the molar flux at the electrode/electrolyte interface of a single particle. When $j = n$ and p, respectively,

$$J_n(t) = \frac{I(t)}{FS_n}, \quad J_p(t) = -\frac{I(t)}{FS_p}. \tag{3}$$

Electrochemical kinetics: The molar flux J_j is governed by the Butler-Volmer equation:

$$J_j(t) = \frac{J_{0,j}}{F}\left[\exp\left(\frac{\alpha_a F}{RT}\eta_j(t)\right) - \exp\left(-\frac{\alpha_c F}{RT}\eta_j(t)\right)\right], \tag{4}$$

where

$$\eta_j(t) = \Phi_{s,j}(t) - \Phi_{e,j}(t) - U(c_{ss,j}(t)) - FR_{f,j}J_j(t).$$

The electrolyte phase can be represented by a resistor $R_{c,j}$ in the SPM, implying $\Phi_{c,j}$ can be expressed as

$$\Phi_{e,j}(t) = R_{c,j}I(t).$$

Hence, η_j becomes

$$\eta_j(t) = \Phi_{s,j}(t) - U(c_{ss,j}(t)) - F\bar{R}_j J_j(t), \tag{5}$$

where $\bar{R}_j = R_{c,j} + R_{f,j}$.

To conclude the model review, the SPM is composed of (1)-(4). A visualization of the relationship between key variables is given in Fig. 2, in which I is the external input, $c_{s,j}$ and $\Phi_{s,j}$ are the variables showing the battery status, and V is the output.

2.3. The Reduced Complexity Model

Average Li$^+$ concentration in the electrode phase: The average concentration of Li$^+$ ions in the particle is considered throughout the paper as the measure of the present battery capacity, or equivalently, the SoC. It is defined as

$$c_{s,j}^{\text{avg}}(t) = \frac{1}{\Omega}\int_\Omega c_{s,j}(r,t)\mathrm{d}\Omega, \tag{6}$$
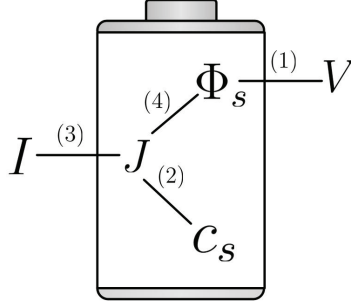
Figure 2: The relationship between key variables in the SPM.

where Ω denotes the volume of the particle sphere. From (2), it is obtained that

$$
\begin{aligned}
\dot{c}_{s,j}^{\text{avg}}(t) &= \frac{1}{\Omega} \int_{\Omega} \frac{\partial c_{s,j}(r,t)}{\partial t} \mathrm{d}\Omega \\
&= \frac{1}{\Omega} \int_{\Omega} \frac{1}{r^2} \frac{\partial}{\partial r} \left(D_{s,j} r^2 \frac{\partial c_{s,j}(r,t)}{\partial r} \right) \mathrm{d}\Omega \\
&= \epsilon_j D_{s,j} \left. \frac{\partial c_{s,j}(r,t)}{\partial r} \right|_{r=\bar{r}_j},
\end{aligned}
\tag{7}
$$

where ϵ_j is a constant coefficient. Depending on the electrode polarity, (7) splits into

$$
\dot{c}_{s,n}^{\text{avg}}(t) = -\frac{\epsilon_n}{FS_n} I(t),
\tag{8}
$$

$$
\dot{c}_{s,p}^{\text{avg}}(t) = \frac{\epsilon_p}{FS_p} I(t).
\tag{9}
$$

By (8)-(9), the rate of change of $c_{s,j}^{\text{avg}}$ is linearly proportional to the input current I. In other words, $c_{s,j}^{\text{avg}}$ is equal to the initial value $c_{s,j}^{\text{avg}}(0)$ plus integration of I over time. This illustrates that the change of SoC depends linearly on I as a result of $c_{s,j}^{\text{avg}}$ indicating SoC. Such a relationship has not only been presented for electrochemical models, e.g., [11], but also justified in ECMs, e.g., [20, 6] and the references therein.

Terminal voltage: Suppose there exists a function φ such that $c_{ss,j}(t) = \varphi(c_{s,j}^{\text{avg}}(t))$ and define $\bar{U} = U \circ \varphi$, where '$\circ$' denotes composition of two functions. Using (5), (1) becomes

$$
V(t) = \bar{U}(c_{s,p}^{\text{avg}}(t)) - \bar{U}(c_{s,n}^{\text{avg}}(t)) + \eta_p(t) - \eta_n(t) + (\bar{R}_p - \bar{R}_n)I(t).
$$

With $\alpha_a = \alpha_c = 0.5$, it follows from (4) that

$$
\begin{aligned}
\eta_n(t) &= \frac{2RT}{F} \sinh^{-1}\left(\frac{J_n(t)F}{2J_{0,n}} \right) = \frac{2RT}{F} \sinh^{-1}\left(\frac{\epsilon_n I(t)}{2J_{0,n}} \right), \\
\eta_p(t) &= \frac{2RT}{F} \sinh^{-1}\left(\frac{J_p(t)F}{2J_{0,p}} \right) = \frac{2RT}{F} \sinh^{-1}\left(-\frac{\epsilon_p I(t)}{2J_{0,p}} \right).
\end{aligned}
$$

7

Thus $V(t)$ becomes

$$V(t) = \bar{U}(c_{s,p}^{\mathrm{avg}}) - \bar{U}(c_{s,n}^{\mathrm{avg}}) + \frac{2RT}{F}\left[\sinh^{-1}\left(-\frac{\epsilon_p I(t)}{2J_{0,p}}\right) - \sinh^{-1}\left(\frac{\epsilon_n I(t)}{2J_{0,n}}\right)\right]$$

$$+ (\bar{R}_p - \bar{R}_n)I(t). \tag{10}$$

As such, V(t) consists of two parts. The first is the open-circuit voltage (OCV) that relies on $\bar{U}(c_{s,j}^{\mathrm{avg}})$, and the second part is the direct feedthrough from I to V.

Construction of the state-space model: It is seen from above that (8)-(10) provide a concise characterization of the battery dynamics. To convert them into a state-space model for SoC estimation, denote the SoC by a state vector $x \in [0,1]$. The input u and the output y of the model can be defined as $u = I$ and $y = V$, respectively. Since $c_{s,j}^{\mathrm{avg}}$ is arguably equivalent to the SoC, the following state-space model can then be constructed on the basis of (8)-(10):

$$\begin{cases} \dot{x}(t) = -au(t), \\ y(t) = h(x(t)) + g(u(t)). \end{cases}$$

In above, $a = \rho/C_n$, where the Coulombic efficiency ρ is a measure of the transfer efficiency of the current charge and C_n is the battery's nominal capacity, $h(\cdot)$ is the counterpart of the part containing $\bar{U}$ in (10), and $g(\cdot)$ corresponds to the part involving I in (10). Discretization of the above system yields

$$\begin{cases} x_{k+1} = x_k - \alpha u_k, \\ y_k = h(x_k) + g(u_k). \end{cases} \tag{11}$$

where $\alpha = aT = \rho T/C_n$ and T is the sampling period.

Note that, $h(\cdot)$ represents the SoC-OCV relationship and thus varies with different batteries. For the battery under consideration, it takes the parametric form as follows:

$$h(x) = \beta_0 \ln(x + \beta_1) + \beta_2.$$

In addition, $g(\cdot)$ can be determined from (10):

$$g(u) = \gamma_0 \left[\sinh^{-1}(\gamma_1 u) - \sinh^{-1}(\gamma_2 u)\right] + \gamma_3 u,$$

where γ_i for $i = 0, 1, 2, 3$ are parameters from (10).

Two reasonable assumptions regarding the model are established. First, based on the well-known charging/discharging properties of Li$^+$ batteries, it is assumed

- **Assumption 1:** the Coulombic efficiency $\rho = 1$ and $y_k \approx h(x_k)$ when the magnitude of the charging/discharging current is low enough.

8

In addition, the precision of the measuring instruments used in our experiments is very high, leading to

- **Assumption 2:** the covariance of the measurement noise is sufficiently small.

An outlook of SoC and parameter estimation: Developed for SoC estimation, the model in (11) contains parameters α, β_i's and γ_i's. Their values are often hard to determine jointly and may even be subject to change over time in practice. It is hence quite appealing to consider 'adaptive SoC estimation' via *simultaneous estimation of the SoC and the unknown parameters*. A two-stage approach can then be designed as follows to realize the notion:

- **Stage 1:** Apply a very small current to charge the battery from zero to full capacity, and then discharge from full to zero. By Assumption 1, the SoC can be directly calculated through integration of the current over time, and the measured output voltage can be regarded as the OCV. Using the SoC-OCV data set collected, the parameters β_i's in $h(\cdot)$ can be determined.

- **Stage 2:** After $h(\cdot)$ is obtained, the state $x(k)$, the parameters α and γ_i's are estimated simultaneously based on the measurements of the charging/discharging current and the output voltage.

This identification problem in Stage 1 can be formulated as a nonlinear least squares data fitting problem, which can be easily addressed by numerical methods such as the Gauss-Newton [21]. Therefore, $h(\cdot)$ is assumed to be known in sequel. More complicated as a nonlinear state and parameter estimation problem, Stage 2 will be the focus of the following study.

3. Joint Observability/identifiability Analysis

Joint observability/identifiability analysis is crucial to state and parameter estimation since it reveals whether effective estimation is possible or not. In this section, it is performed using the approach of sensitivity analysis.

The identifiability problem: The joint observability/identifiability problem is tackled by parameter identifiability analysis by transforming the model in (11) into the model including the initial state and the parameters:

$$y_k = \phi(\boldsymbol{\theta}; u_0, \cdots, u_k), \tag{12}$$

where

$$\boldsymbol{\theta} = \begin{bmatrix} x_0 & \alpha & \gamma_0 & \gamma_1 & \gamma_2 & \gamma_3 \end{bmatrix}^{\mathrm{T}},$$

$$\phi(\boldsymbol{\theta}; u_0, \cdots, u_k) = h\left(x_0 + \alpha \sum_{i=0}^{k-1} u_i\right) + g(u_k, \gamma).$$

In sequel, $\boldsymbol{\theta}_i$ for $i = 1, 2, \cdots, 6$ and its corresponding parameter will be used interchangeably. Thus the identifiability problem for (12) is: given the data set $\mathcal{Z}_N = \{u_0, \cdots, u_N, y_0, \cdots, y_N\}$, can $\boldsymbol{\theta}$ be uniquely identified? If it cannot be, which parameters in $\boldsymbol{\theta}$ can be identified, and what is the difficulty to determine each parameter?

Before proceeding further, it is important to introduce a definition of local identifiability following [22]:

Definition 1. *A model structure $\phi(\boldsymbol{\theta}; u_0, \cdots, u_k)$ is said to be locally identifiable in some point $\boldsymbol{\theta}_0$ in the parameter space for a given $\{u_0, u_1, \cdots, u_N\}$, if for any $\boldsymbol{\theta}^1$ and $\boldsymbol{\theta}^2$ within the neighborhood of $\boldsymbol{\theta}^0$, $\phi(\boldsymbol{\theta}^1; u_0, \cdots, u_k) = \phi(\boldsymbol{\theta}^2; u_0, \cdots, u_k)$ holds if and only if $\boldsymbol{\theta}^1 = \boldsymbol{\theta}^2$.*

Basics of sensitivity analysis: Sensitivity analysis is used to investigate the identifiability of $\boldsymbol{\theta}$ through investigating the sensitivity of y_k with respect to the change of $\boldsymbol{\theta}$. The sensitivity matrix for (12) is given by

$$\mathbf{S}(\boldsymbol{\theta}) = \begin{bmatrix} & \vdots & \\ \cdots & s_{ki} & \cdots \\ & \vdots & \end{bmatrix}, \tag{13}$$

where

$$s_{ki} = \frac{\partial y_k}{\partial \boldsymbol{\theta}_i}$$

for $k = 0, 1, \cdots, N$ and $i = 1, 2, \cdots, 6$.

To estimate $\boldsymbol{\theta}$, consider the following weighted mean-square-error cost function without loss of generality:

$$\ell(\boldsymbol{\theta}) = \frac{1}{2} \sum_{i=0}^{N} w_i \delta_i^2(\boldsymbol{\theta}) = \frac{1}{2} \boldsymbol{\Delta}^{\mathrm{T}} \mathbf{W} \boldsymbol{\Delta},$$

where $w_i > 0$, $\delta_i = y_i - \phi(\boldsymbol{\theta}; u_0, \cdots, u_i)$, $\boldsymbol{\Delta} = [\delta_0 \cdots \delta_N]^{\mathrm{T}}$, and $\mathbf{W} = \mathrm{diag}(w_0, \cdots, w_N)$. Here, $\mathbf{W}$ can be viewed as a weight matrix to account for the effects of the measurement noise. By Assumption 2, the diagonal elements of $\mathbf{W}$ are relatively large.

The best estimate of $\boldsymbol{\theta}$, denoted as $\hat{\boldsymbol{\theta}}$, is the one that minimizes $\ell(\boldsymbol{\theta})$, that is,

$$\min_{\boldsymbol{\theta}} \ell(\boldsymbol{\theta}) = \ell(\hat{\boldsymbol{\theta}}).$$

10

It is known that $\hat{\boldsymbol{\theta}}$ will be the locally unique solution to minimize $\ell(\boldsymbol{\theta})$ if $\ell'(\hat{\boldsymbol{\theta}}) = 0$ and $\ell''(\hat{\boldsymbol{\theta}}) > 0$. Note that the Hessian $\ell''(\boldsymbol{\theta})$ is

$$\ell''(\boldsymbol{\theta}) = \mathbf{S}^{\mathrm{T}}(\boldsymbol{\theta})\mathbf{W}\mathbf{S}(\boldsymbol{\theta}) - \sum_{i=0}^{N} \boldsymbol{\Delta}^{\mathrm{T}}\mathbf{W}_i \frac{\partial}{\partial \boldsymbol{\theta}} \left(\frac{\partial \phi(\boldsymbol{\theta}; u_0, \cdots, u_i)}{\partial \boldsymbol{\theta}} \right)^{\mathrm{T}},$$

where $\mathbf{W}_i$ is the i-th column of $\mathbf{W}$. When $\boldsymbol{\theta} = \hat{\boldsymbol{\theta}}$, the second term in the right hand side becomes negligible because $\boldsymbol{\Delta}$ approaches zero. Thus $\ell''(\hat{\boldsymbol{\theta}})$ can be approximately rewritten as

$$\ell''(\boldsymbol{\theta}) \approx \mathbf{S}^{\mathrm{T}}(\boldsymbol{\theta})\mathbf{W}\mathbf{S}(\boldsymbol{\theta}). \qquad (14)$$

From (14), it is seen that $\ell''(\hat{\boldsymbol{\theta}}) > 0$ if and only if $\mathbf{S}(\hat{\boldsymbol{\theta}})$ has full column rank.

Local identifiability analysis of $\boldsymbol{\theta}$: For the battery model in (11), the sensitivity coefficients are given by

$$s_{k1} = \frac{\beta_0}{x_0 + \alpha \sum_{i=0}^{k-1} u_i + \beta_1},$$

$$s_{k2} = -\frac{\beta_0 \sum_{i=0}^{k-1} u_i}{x_0 + \alpha \sum_{i=0}^{k-1} u_i + \beta_1},$$

$$s_{k3} = \sinh^{-1}(\gamma_1 u_k) - \sinh^{-1}(\gamma_2 u_k),$$

$$s_{k4} = \frac{\gamma_0 u_k}{\sqrt{\gamma_1^2 u_k^2 + 1}},$$

$$s_{k5} = -\frac{\gamma_0 u_k}{\sqrt{\gamma_2^2 u_k^2 + 1}},$$

$$s_{k6} = u_k.$$

The order of magnitude of each variable is: $x_0 \approx 10^{-1}$, $\alpha \approx 10^{-5}$, $\beta_0 \approx 10^0$, $\beta_1 \approx 10^0$, $\beta_2 \approx 10^0$, $\gamma_0 \approx 10^{-2}$, $\gamma_1 \approx -(10^{-7} \sim 10^{-6})$, $\gamma_2 \approx 10^{-7} \sim 10^{-6}$ and $\gamma_3 \approx 10^{-3} \sim 10^{-2}$. Suppose u_k lies within the reasonable range of $-20 \sim 20$.

The degree of influence of the change in $\boldsymbol{\theta}_i$ on y_k can not be fully shown by the sensitivity s_{ki} for $i = 1, 2, \cdots, 6$, because it is also dependent on the scale of $\boldsymbol{\theta}_i$. Thus s_{ki} should be normalized to eliminate the scale-induced effects:

$$s_{ki}^* = |\boldsymbol{\theta}_i| \, s_{ki},$$

from which the normalized sensitivity matrix $\mathbf{S}^*$ can be defined accordingly. The normalized Hessian H^* is defined as

$$\mathbf{H}^*(\boldsymbol{\theta}) = \boldsymbol{\Gamma}_{\boldsymbol{\theta}} \ell''(\boldsymbol{\theta}) \boldsymbol{\Gamma}_{\boldsymbol{\theta}}$$

11

$$= \mathbf{S}^{*\mathrm{T}}(\boldsymbol{\theta})\mathbf{W}\mathbf{S}^*(\boldsymbol{\theta}),$$

where $\boldsymbol{\Gamma_\theta} = \mathrm{diag}(|\boldsymbol{\theta}_1|, \cdots, |\boldsymbol{\theta}_6|)$. Analysis of s_{ki}^* and S^* establishes the following:

Fact 1. *The parameter vector $\boldsymbol{\theta}$ is almost locally unidentifiable.*

Explanation of this fact is straightforward. It is seen that $s_{ki}^* \to 0$ for $i = 3, 4, 5$. This indicates that $\mathbf{S}_i^*$ for $i = 3, 4, 5$, where $\mathbf{S}_i^*$ is the i-th column of $\mathbf{S}^*$, are almost linearly dependent. From a theoretical perspective, if $\{u_k\}$ contains a rich mix of frequency contents, $\mathbf{S}_2^*$ corresponding to α is independent of the other $\mathbf{S}_i^*$'s. However, the order of magnitude of s_{k2}^* is quite small, which lies between $10^{-5} \sim 10^{-1}$, depending on the scale of $\{u_k\}$. It can be concluded that $\mathbf{S}^*$ will be almost surely rank-deficient in numerical sense, with rank of about 3, so $\boldsymbol{\theta}$ can be hardly identified.

It is now worth considering what can be identified using the given model and data even if $\boldsymbol{\theta}$ cannot be identified as a whole. It is pointed out in [22] that a reparameterized model structure, or more specifically, a combination of parameters in $\boldsymbol{\theta}$, can be identified. The next remarkable fact is established.

Fact 2. *Despite Fact 1, x_0 can still be locally identified with high accuracy.*

Intuitive thinking shows that x_0 can still be estimated due to the independence of $\mathbf{S}_1^*$ from $\mathbf{S}_i^*$ for $i = 2, \cdots, 6$ and the order of magnitude of s_{k1}^* far exceeding s_{ki}^* for $i = 2, \cdots, 6$. An additional support is that x_k is noted to be the major force that causes the increasing/decreasing values of y_k during the charging/discharging processes. Now consider the normalized Hessian $\mathbf{H}^*$, which is rank deficient. Its singular value decomposition (SVD) can be expressed by

$$\mathbf{H}^* = \begin{bmatrix} \mathbf{U}_l & \mathbf{U}_s \end{bmatrix} \begin{bmatrix} \boldsymbol{\Sigma}_l & \mathbf{0} \\ \mathbf{0} & \mathbf{0} \end{bmatrix} \begin{bmatrix} \mathbf{V}_l^{\mathrm{T}} \\ \mathbf{V}_s^{\mathrm{T}} \end{bmatrix}, \qquad (15)$$

where $\mathbf{U}$ and $\mathbf{V}$ are unitary matrices and $\boldsymbol{\Sigma}_l$ is a diagonal matrix containing nonzero singular values of $\mathbf{H}^*$. The rank of $\mathbf{H}^*$ is 3 since $\mathbf{S}^*$ has rank 3 as aforementioned. Hence, the dimensions of $\boldsymbol{\Sigma}_l$, $\mathbf{U}_l$ and $\mathbf{V}_l$ are 3×3, 6×3 and $6 \times x$, respectively. It can be proven that the column space of $\mathbf{U}_l$ is the subspace of the identifiable parameter space [22]. In other words, the vector $\boldsymbol{\vartheta}$ obtained from reparameterizing $\boldsymbol{\theta}$ is identifiable, where $\boldsymbol{\vartheta}$ is given by

$$\boldsymbol{\vartheta} = \mathbf{U}_l^{\mathrm{T}}\boldsymbol{\theta}. \qquad (16)$$

It is of much importance to note that an element in $\boldsymbol{\vartheta}$ will correspond to $\boldsymbol{\theta}_1$ or x_0 with extremely minor difference due to the numerical properties of $\mathbf{S}^*$ given above. That is,

x_0 will be projected by $\mathbf{U}_l$ to a point in the identifiable subspace, which is very close to itself. Thus it can be identified with a considerable amount of accuracy. A simulation-based identifiability study will be given in Example 1 of Section 5 to validate the findings presented.

According to the analysis, a joint state and parameter estimation algorithm can be designed, which, though only able to yield imprecise estimates for α and γ_i's, would still provide reliable SoC estimates. Hence, adaptive SoC estimation is achievable. However, this requires model restructuring.

As can be seen from the above, the term $\gamma_0 \left[\sinh^{-1}(\gamma_1 u) - \sinh^{-1}(\gamma_2 u)\right]$ plays a role that can be neglected in the measurement equation of the model (11). Therefore, a further simplified battery model may be used via reducing $g(u)$ as $g(u) = \gamma u$:

$$
\begin{cases}
x_{k+1} = x_k - \alpha u_k, \\
y_k = \beta_0 \ln(x_k + \beta_1) + \beta_2 + \gamma u_k.
\end{cases}
\tag{17}
$$

The parameter vector $\boldsymbol{\theta}$ of this model is

$$
\boldsymbol{\theta} = \begin{bmatrix} x_0 & \alpha & \gamma \end{bmatrix}^{\mathrm{T}}.
$$

The following facts regarding (17) can be stated:

Fact 3. *For the model* (17), *$\boldsymbol{\theta}$ is locally identifiable when the input sequence $\{u_k\}$ contains a sufficiently rich mix of frequency contents.*

Fact 4. *Among all the parameters, x_0 is the 'easiest' one to estimate.*

Here, the normalized sensitivity matrix $\mathbf{S}^*(\boldsymbol{\theta})$ is given by

$$
\mathbf{S}^*(\boldsymbol{\theta}) = \begin{bmatrix}
\vdots & \vdots & \vdots \\
\dfrac{|x_0|\beta_0}{x_0 + \alpha \sum_{i=0}^{k-1} u_i + \beta_1} & -\dfrac{|\alpha|\beta_0 \sum_{i=0}^{k-1} u_i}{x_0 + \alpha \sum_{i=0}^{k-1} u_i + \beta_1} & |\gamma| u_k \\
\vdots & \vdots & \vdots
\end{bmatrix}
$$

Fact 3 is straightforward following the similar lines to analyze the full rankness of $\mathbf{S}^*$. 'Easiest' in Fact 4 means that the estimate of the parameter x_0 has the smallest error covariance. It is known that

$$
\begin{aligned}
\mathrm{Cov}(\boldsymbol{\Gamma}_{\boldsymbol{\theta}}^{-1}\hat{\boldsymbol{\theta}}) &\approx \left[\mathrm{E}\left(\mathbf{H}^*(\hat{\boldsymbol{\theta}})\right)\right]^{-1} \\
&= \left[\mathrm{E}\left(\mathbf{S}^{*\mathrm{T}}(\hat{\boldsymbol{\theta}})\mathbf{W}\mathbf{S}^*(\hat{\boldsymbol{\theta}})\right)\right]^{-1}.
\end{aligned}
$$

13

Consider diag $\left[\mathrm{Cov}(\mathbf{\Gamma}_{\boldsymbol{\theta}}^{-1}\hat{\boldsymbol{\theta}}) \right]$, which indicates the error covariance of $\hat{\boldsymbol{\theta}}$. Its first element corresponding to x_0 will be much smaller than the others, because the elements of $\mathbf{S}_1^*$ has much larger magnitudes than those of $\mathbf{S}_2^*$ and $\mathbf{S}_3^*$. Fact 4 will also be validated in Example 1 of Section 5.

4. Adaptive SoC Estimation

The adaptive SoC estimation is treated as joint state and parameter estimation. In this section, an IEKF-based technique will developed for the model (17). The IEKF is an improved version of the KF and EKF to deal with severe nonlinearities in the system by iteratively refining the state estimate around the current point at each time instant. Its estimation performance is superior to the EKF, while the increase in computational complexities can be restrained to a tolerable level.

State augmentation: To use the IEKF, define an augmented state vector to incorporate both the original state x and the unknown parameters:

$$\boldsymbol{\xi}_k = \begin{bmatrix} x_k & \alpha & \gamma \end{bmatrix}^{\mathrm{T}}.$$

Analogous to $\boldsymbol{\theta}$, $\boldsymbol{\xi}_{i,k}$ for $i = 1, 2, 3$ and its corresponding variable or parameter will be used interchangeably. Thus (11) can be rewritten as

$$\begin{cases} \boldsymbol{\xi}_{k+1} = \mathbf{F}_k \boldsymbol{\xi}_k, \\ y_k = \bar{h}(\boldsymbol{\xi}_k, u_k), \end{cases} \tag{18}$$

where

$$\mathbf{F}_k = \begin{bmatrix} 1 & u_k & \\ & 1 & \\ & & 1 \end{bmatrix},$$

$$\bar{h}(\boldsymbol{\xi}_k) = \beta_0 \log(\boldsymbol{\xi}_{1,k} + \beta_1) + \beta_2 + \boldsymbol{\xi}_{3,k} u_k.$$

Application of the IEKF: For the augmented battery model in (18), the IEKF is applied to estimating $\boldsymbol{\xi}_k$. Like the KF and EKF, it consists of two procedures — prediction and update.

The prediction formulae of the IEKF are

$$\hat{\boldsymbol{\xi}}_{k|k-1} = \mathbf{F}_{k-1}\hat{\boldsymbol{\xi}}_{k-1|k-1}, \tag{19}$$

$$\mathbf{P}_{k|k-1} = \mathbf{F}_{k-1}\mathbf{P}_{k-1|k-1}\mathbf{F}_{k-1}^{\mathrm{T}} + \mathbf{Q}, \tag{20}$$

14

where $\hat{\boldsymbol{\xi}}_{k|k-1}$ and $\hat{\boldsymbol{\xi}}_{k|k}$ are the estimates of $\boldsymbol{\xi}_k$ given $\mathcal{Z}_{k-1}$ and $\mathcal{Z}_k$, respectively, $\mathbf{P}$ is the estimation error covariance, and $\mathbf{Q} \geq 0$ is adjustable to reduce the effects of process noise.

The update is implemented iteratively:

$$\mathbf{K}_k^{(i)} = \mathbf{P}_{k|k-1} H_k^{(i-1)} \left[\mathbf{H}_k^{(i-1)} \mathbf{P}_{k|k-1} \mathbf{H}_k^{(i-1)\mathrm{T}} + R \right]^{-1}, \tag{21}$$

$$\hat{y}_k^{(i)} = \bar{h}(\hat{\boldsymbol{\xi}}_{k|k}^{(i-1)}), \tag{22}$$

$$\hat{\boldsymbol{\xi}}_{k|k}^{(i)} = \hat{\boldsymbol{\xi}}_{k|k-1} + \mathbf{K}_k^{(i)} \left[y_k - \hat{y}_k^{(i)} - \mathbf{H}_k^{(i-1)}(\hat{\boldsymbol{\xi}}_{k|k-1} - \hat{\boldsymbol{\xi}}_{k|k}^{(i-1)}) \right], \tag{23}$$

where $R > 0$, the superscript (i) denotes the iteration number, $\hat{\boldsymbol{\xi}}_{k|k}^{(0)} = \hat{\boldsymbol{\xi}}_{k|k-1}$ and

$$\mathbf{H}_k^{(i)} = \left. \frac{\partial \bar{h}}{\partial \boldsymbol{\xi}} \right|_{\hat{\boldsymbol{\xi}}_{k|k}^{(i)}}.$$

The iteration process stops when i achieves the pre-specified maximum iteration number $i_{\max}$ or when the error between two consecutive iterations is less than the pre-selected tolerance level. The associated estimation error covariance is given by

$$\mathbf{P}_{k|k} = (\mathbf{I} - \mathbf{K}_k^{(i_{\max})} \mathbf{H}_k^{(i_{\max})}) \mathbf{P}_{k|k-1}. \tag{24}$$

The estimate of SoC at time instant k is then given by $\hat{\boldsymbol{\xi}}_{1,k}^{(i_{\max})}$.

The IEKF-based adaptive SoC estimation algorithm, `AdaptSoC`, is summarized in (19)-(24). It has a recursive structure for sequential real-time implementation, and furthermore, the update procedure is executed through iterative operations.

Discussion: Regarding the `AdaptSoC`, the following remarks are given:

Remark 1. Convergence of `AdaptSoC`. *Convergence analysis for the nonlinear joint state and parameter estimation considered is difficult to perform. The discussion in [23] may shed some light, which is about the convergence properties of the EKF for joint parameter and state estimation problem for linear systems. It is shown in [23] that the estimates may be biased because of the lack of coupling between the filtering gain and the parameters. While likely to suffer from the similar bias problem to a certain extent, AdaptSoC should have better convergence performance, because the IEKF is numerically more accurate than the EKF and the noise level in our experiments is quite low.*

Remark 2. Feasible improvements to `AdaptSoC`. *The update procedure of IEKF is equivalent to applying the Gauss-Newton method to finding the minimum of a mean-square-error cost function [24]. There are a few methods available in the literature as improvements of the Gauss-Newton method, e.g., the Levenberg-Marquardt algorithm with better convergence properties and numerical stability. They can be used in the AdaptSoC to attain better estimation performance.*

Remark 3. Potential alternatives to `AdaptSoC`. *Essentially, the `AdaptSoC` is concerned with joint state and parameter estimation using state augmentation and the IEKF. Its development is motivated by conceptual simplicity, satisfactory SoC estimation performance validated by experiments and modest computational complexity. However, there exist a few other alternatives to choose from. Not only can other state estimation techniques such as UKF, particle filter and nonlinear Gaussian filter substitute the IEKF, but various methods for joint state and parameter estimation, e.g. [25, 26], can also be potentially used here.*

5. Application Studies

Three examples are given to verify the findings and effectiveness of `AdaptSoC`. The first two are based on numerical simulation, and the third uses experimental data.

Example 1. Identifiability analysis. *Consider the model in* (11) *and assume that it is accurate. The nominal parameter values are given as follows:* $\alpha = 5.0708 \times 10^{-5}$, $\beta_0 = 1.0480$, $\beta_1 = 2.208 \times 10^{-1}$, $\beta_2 = 3.9998$, $\gamma_0 = 5.1400 \times 10^{-2}$, $\gamma_1 = 8.7615 \times 10^{-7}$, $\gamma_2 = -1.5274 \times 10^{-7}$, $\gamma_3 = -5 \times 10^{-3}$. *The values of* α *and* γ_i*'s are reckoned according to [18, 19]. The values of* β_i*'s are determined by fitting the SoC-OCV data of the battery that will be experimented with in Example 3. The weight matrix* $\mathbf{W} = 10^8 \mathbf{I}$. *The input to the model is a square wave alternating between* $5A$ *and* $-5A$ *with period of* $40s$ *for* 100 *cycles.*

Let us verify Fact 2 in the first place. According to the results in Section 3, the normalized Hessian around the above nominal parameters can be computed:

$$
\mathbf{H}^* = \begin{bmatrix}
2.0992 \times 10^{11} & 1.0619 \times 10^9 & 1.3429 \times 10^1 & 1.1435 \times 10^1 & -1.9935 \times 10^0 & 1.2696 \times 10^6 \\
1.0619 \times 10^9 & 7.1804 \times 10^6 & -1.9359 \times 10^1 & -1.6485 \times 10^1 & 2.8738 \times 10^0 & -1.8303 \times 10^6 \\
1.3429 \times 10^1 & -1.9359 \times 10^1 & 2.7968 \times 10^{-2} & 2.3816 \times 10^{-2} & -4.1519 \times 10^{-3} & 2.6442 \times 10^3 \\
1.1435 \times 10^1 & -1.6485 \times 10^1 & 2.3816 \times 10^{-2} & 2.0281 \times 10^{-2} & -3.5356 \times 10^{-3} & 2.2517 \times 10^3 \\
-1.9935 \times 10^0 & 2.8738 \times 10^0 & -4.1519 \times 10^{-3} & -3.5356 \times 10^{-3} & 6.1636 \times 10^{-4} & -3.9254 \times 10^2 \\
1.2696 \times 10^6 & -1.8303 \times 10^6 & 2.6442 \times 10^3 & 2.2517 \times 10^3 & -3.9254 \times 10^2 & 2.5000 \times 10^8
\end{bmatrix}.
$$

By SVD, the singular values of $\mathbf{H}^*$ *listed in decreasing order are*

$$
\sigma_1 = 2.0992 \times 10^{11}, \sigma_2 = 2.5001 \times 10^8, \sigma_3 = 1.7945 \times 10^6,
$$
$$
\sigma_4 = 1.9497 \times 10^{-13}, \sigma_5 = 6.1746 \times 10^{-16}, \sigma_6 = 2.2716 \times 10^{-17}.
$$

Direct observation shows that the singular values vary dramatically in magnitude. In particular, the last three singular values are ignorable, so the rank of $\mathbf{H}^*$ *is 3. As in* (15)*,* $\mathbf{U}_l$ *corresponding to the three largest eigenvalues in this case is*

$$
\mathbf{U}_l = \begin{bmatrix}
9.9999 \times 10^{-1} & -3.1423 \times 10^{-5} & -5.0588 \times 10^{-3} \\
5.0589 \times 10^{-3} & 7.3996 \times 10^{-3} & 9.9996 \times 10^{-1} \\
6.3578 \times 10^{-11} & -1.0577 \times 10^{-5} & 7.8266 \times 10^{-8} \\
5.4140 \times 10^{-11} & -9.0066 \times 10^{-6} & 6.6647 \times 10^{-8} \\
-9.4383 \times 10^{-12} & 1.5701 \times 10^{-6} & -1.1619 \times 10^{-8} \\
6.0110 \times 10^{-6} & -9.9997 \times 10^{-1} & 7.3996 \times 10^{-3}
\end{bmatrix}
$$
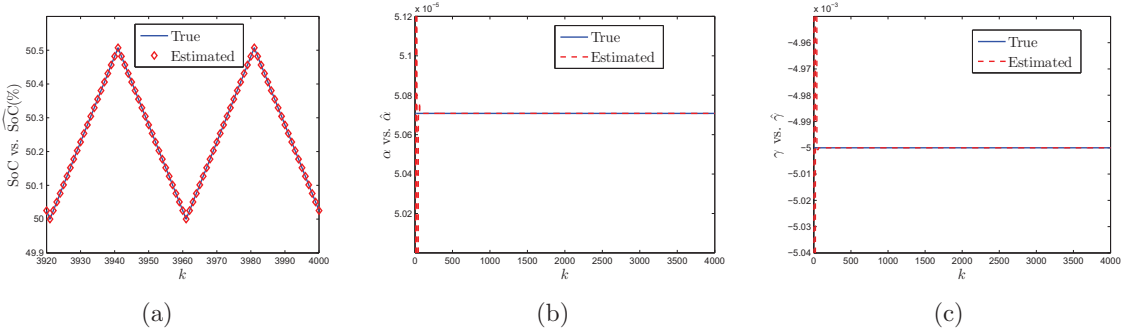
Figure 3: Example 2 — noise-free case: (a) SoC estimation; (b) estimation of α; (c) estimation of γ.

Using (16), the identifiable vector ϑ repameterized from $\boldsymbol{\theta}$ can be obtained via the unitary projection matrix $\mathbf{U}_l$. Here, $\vartheta_1 = \mathbf{U}_{l,1}^{\mathrm{T}}\boldsymbol{\theta}$, where $\mathbf{U}_{l,1}$ is the first column of $\mathbf{U}_l$. It follows immediately that

$$\begin{aligned}
\vartheta_1 &= 9.9999 \times 10^{-1}x_0 + 5.0589 \times 10^{-3}\alpha + 6.3578 \times 10^{-11}\gamma_0 \\
&\quad + 5.4140 \times 10^{-11}\gamma_1 - 9.4383 \times 10^{-12}\gamma_2 + 6.0110 \times 10^{-6}\gamma_3 \\
&\approx x_0,
\end{aligned}$$

because the magnitude of x_0 far exceeds those of α and γ_i's for $i = 0, 1, \cdots, 3$. Thus Fact 2 is verified.

Now consider the verification of Fact 4. The model (17) is used, where $\gamma = -5 \times 10^{-3}$. Let $\hat{\boldsymbol{\theta}}$ take the true parameter values for simulation purpose. The normalized identification error covariance matrix is given by

$$\mathrm{Cov}(\boldsymbol{\Gamma}_{\boldsymbol{\theta}}^{-1}\hat{\boldsymbol{\theta}}) = \begin{bmatrix} 1.9024 \times 10^{-11} & 2.8188 \times 10^{-9} & -2.0734 \times 10^{-11} \\ 2.8188 \times 10^{-9} & 5.5720 \times 10^{-7} & -4.0936 \times 10^{-9} \\ -2.0734 \times 10^{-11} & -4.0936 \times 10^{-9} & 4.0301 \times 10^{-9} \end{bmatrix}.$$

It is seen from above that the normalized error covariance of $\hat{\boldsymbol{\theta}}_1$ or $\hat{x}_0$ is the smallest and much less than that of $\hat{\alpha}$ and $\hat{\gamma}$, thus validating Fact 4.

Example 2. Application of `AdaptSoC` to a perfect model. *Consider the model in (17) with the same parameters and input sequence as in Example 1. The noise-free case is investigated first. The input data is applied to the model to generate the output using (17). Then* `AdaptSoC` *is implemented to process the input and output data to estimate the SoC. The iteration number at each time step is set to be 10 in the update procedure. The initial actual SoC is 50%, and the initial SoC estimate takes the value of 40%. The estimation results are shown in Fig. 3. It is illustrated that the estimates of the SoC, α and γ coincide with the true values after a few seconds. The almost fully accurate state and parameter estimation*

17
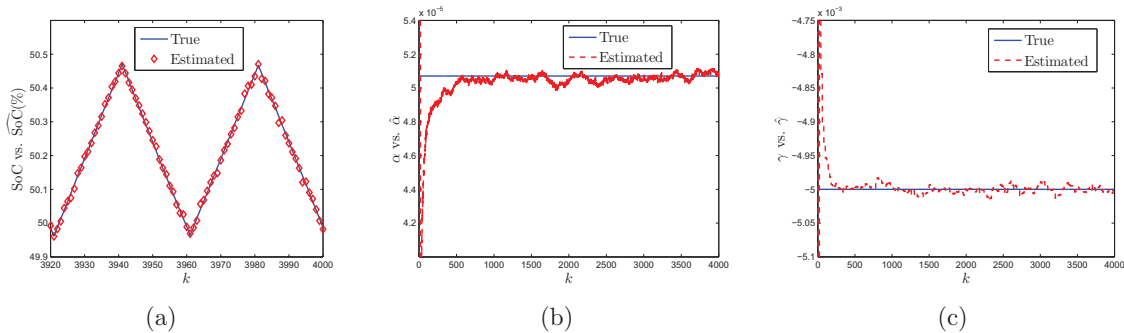
Figure 4: Example 2 — noisy case: (a) SoC estimation; (b) estimation of α; (c) estimation of γ.

for systems without noise corruption supports the finding that the model parameter vector is locally identifiable as stated in Fact 3.

A weak white noise process with covariance of 10^{-8} is added to the measured output to account for practical limitation. We follow the same procedure as above and apply `AdaptSoC` to the simulation data to estimate the SoC, α and γ. The overall estimation performance, as shown in Fig. 4, deteriorates as a result of the measurement noise, with the estimates slightly differing from the actual values. Visual comparison indicates that the estimation of α and γ is relatively poor compared to the SoC. This corroborates Fact 4 and the computational analysis in Example 1, both of which argue that the SoC is easier to estimate than α and γ.
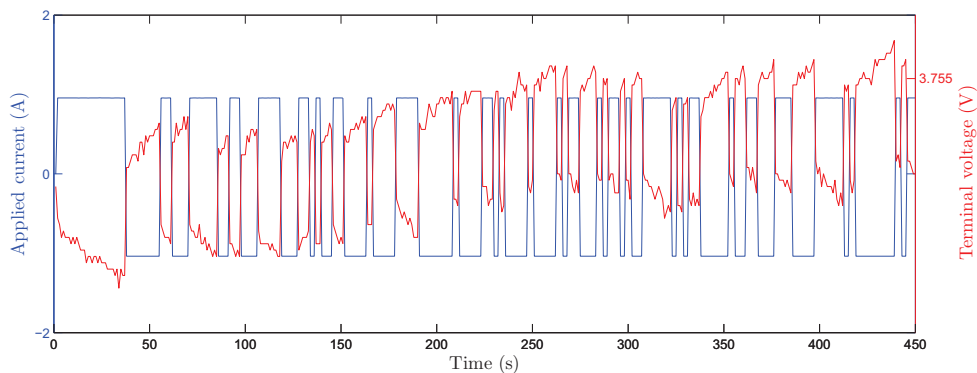
Figure 5: Example 3: the input-output (current-voltage) profile.

Example 3. Application of `AdaptSoC` to experimental data. *To evaluate the real-world performance of* `AdaptSoC`, *data was collected from a Li^{+} battery via practical experiments. No details regarding the battery could be released due to required intellectual property protection.*

In this experiment, the SoC-OCV relationship was obtained at the first stage, and the values of β_i's were identified using nonlinear least squares fitting from the SoC-OCV data.

18
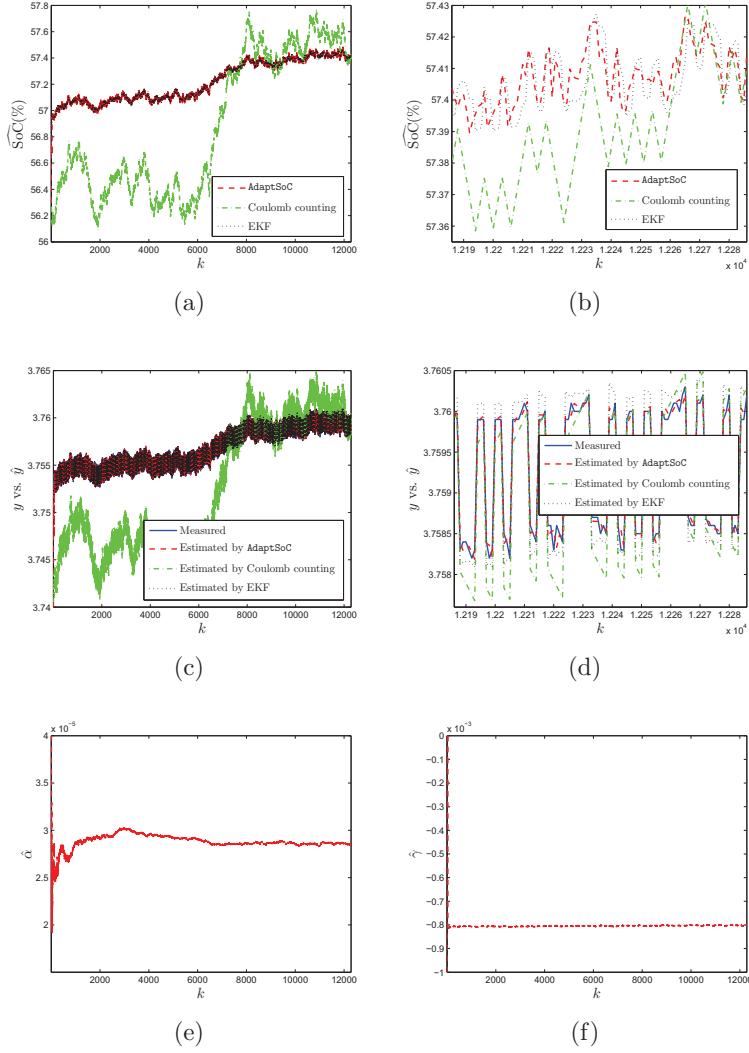
Figure 6: Example 3: (a) SoC estimation; (b) SoC estimation output in a partially enlarged view; (c) output estimation; (d) output estimation in a partially enlarged view; (e) estimation of α; (f) estimation of γ.

*Then **AdaptSoC** was implemented to estimate the SoC from the current-voltage data during the second stage. For comparison purpose, the Coulomb counting and non-adaptive EKF reported in the literature were also applied to the data for SoC estimation.*

The current applied is a pseudo-random binary signal (PRBS) that is stretched by 10 times over the time axis and alternates between approximately 1A and -1A. A PRBS signal is periodic, deterministic, but has white-noise-like properties, so it is commonly used in system identification [27]. The resultant current-voltage profile within the first 450s is shown in Fig. 5. With some a priori knowledge of the experiment, it was understood that the initial

SoC was roughly 50%, so the initial SoC estimate is set to be 56.3%.

An overview of SoC estimation through time is illustrated in Fig. 6(a). The SoC estimates given by Coulomb counting are significantly different from those by **AdaptSoC** *and EKF, while an enlarged view in Fig. 6(b) shows milder difference between the latter two. The actual SoC values cannot be measured due to equipment limitations, but we can compare the true output $\{y_k\}$ with the predicted one $\{\hat{y}_{k|k-1}\}$ for an indirect analysis of the SoC estimation accuracy. Here, one-step-ahead prediction is used, e.g., $\hat{y}_{k|k-1} = \bar{h}(\hat{\boldsymbol{\xi}}_{k|k-1})$ in the case of* **AdaptSoC***, please refer to (18). It is seen from Fig. 6(c) that the predicted output resulting from Coulomb counting deviates from the measured data. From partial enlargement given in Fig. 6(d), it is observed that* **AdaptSoC** *leads to excellent output prediction. Compared with the EKF, it has much smaller output prediction error. This suggests considerable confidence on* **AdaptSoC***-based SoC estimation.*

In addition, the following consistent observations are obtained through numerous simulations:

- *Coulomb counting is sensitive to the initial SoC estimate and tends to be less accurate due to lack of correction using the output data;*

- *EKF may exhibit satisfactory SoC estimation, largely depending on the accuracy of parameter values, but the parameters are often difficult to be determined precisely due to battery dynamics involving uncertainty and variation over time.*

- **AdaptSoC***, unlike Coulomb counting and EKF, yields reliable SoC estimation results with robustness to initial estimate and even in the presence of unknown parameters.*

While **AdaptSoC** *only guarantees effective SoC estimation, estimation of the parameters α and γ over time is depicted in Fig. 6(e)-6(f). Despite its relatively lower accuracy as analyzed in Section 3 and demonstrated in Example 1, the parameter estimation may still provide some clues to practitioners on the parameters.*

From the above analysis, we see that **AdaptSoC** *is a promising method with much potential for practical application. Taking full advantage of the input-output data, it does not require high-accuracy initial SoC estimate and model parameters but is still able to provide effective SoC estimation.*

6. Conclusion

SoC estimation is of much importance for safe and efficient application of Li^+ as energy storage devices in various areas. The design of SoC estimators usually follow the trilogy of 'modeling—identification—SoC estimation'. This paper, however, studies *adaptive SoC estimation* for Li^+ batteries, which integrates SoC estimation with parameter identification. A reduced-complexity model is derived from the single particle model. Joint observability/identifiability of the SoC and the unknown parameters of the model is investigated,

showing the advantageous property that the SoC is almost locally observable. An iterated extended Kalman filter-based adaptive SoC estimator, the `AdaptSoC` algorithm, is then developed. The analysis results and the effectiveness of `AdaptSoC` are verified by both simulation and experiments. Due to its excellent estimation performance and easy implementation, `AdaptSoC` will hopefully have strong practical appeal.

References

[1] Y. Nishi, Lithium ion secondary batteries; past 10 years and the future, Journal of Power Sources 100 (1-2) (2001) 101–106.

[2] N. Chaturvedi, R. Klein, J. Christensen, J. Ahmed, A. Kojic, Algorithms for advanced battery-management systems, IEEE Control Systems Magazine 30 (3) (2010) 49–68.

[3] V. Pop, H. J. Bergveld, P. H. L. Notten, P. P. L. Regtien, State-of-the-art of battery state-of-charge determination, Measurement Science and Technology 16 (12) (2005) R93–R110.

[4] S. Piller, M. Perrin, A. Jossen, Methods for state-of-charge determination and their applications, Journal of Power Sources 96 (1) (2001) 113–120.

[5] J. Chiasson, B. Vairamohan, Estimating the state of charge of a battery, IEEE Transactions on Control Systems Technology 13 (3) (2006) 465–470.

[6] G. L. Plett, Extended Kalman filtering for battery management systems of LiPB-based HEV battery packs: Part 3. State and parameter estimation, Journal of Power Sources 134 (2) (2004) 277–292.

[7] G. L. Plett, Sigma-point Kalman filtering for battery management systems of LiPB-based HEV battery packs: Part 2: Simultaneous state and parameter estimation, Journal of Power Sources 161 (2) (2006) 1369–1384.

[8] I.-S. Kim, The novel state of charge estimation method for lithium battery using sliding mode observer, Journal of Power Sources 163 (1) (2006) 584–590.

[9] M. Verbrugge, E. Tate, Adaptive state of charge algorithm for nickel metal hydride batteries including hysteresis phenomena, Journal of Power Sources 126 (1-2) (2004) 236–249.

[10] Y. Hu, S. Yurkovich, Battery cell state-of-charge estimation using linear parameter varying system techniques, Journal of Power Sources 198 (2012) 338–350.

[11] K. A. Smith, C. D. Rahn, C.-Y. Wang, Model-based electrochemical estimation of Lithium-ion batteries, in: Proceedings of IEEE International Conference on Control Applications, 2008, pp. 714–719.

[12] D. Domenico, G. Di Fiengo, A. Stefanopoulou, Lithium-ion battery state of charge estimation with a Kalman filter based on a electrochemical model, in: Proceedings of IEEE International Conference on Control Applications, 2008, pp. 702–707.

[13] S. Santhanagopalan, R. E. White, State of charge estimation using an unscented filter for high power lithium ion cells, International Journal of Energy Research 34 (2) (2010) 152–163.

[14] R. Klein, N. Chaturvedi, J. Christensen, J. Ahmed, R. Findeisen, A. Kojic, Electrochemical model based observer design for a Lithium-ion battery, IEEE Transactions on Control Systems Technology 21 (2) (2013) 289–301.

[15] S. J. Moura, N. A. Chaturvedi, M. Krstic, PDE estimation techniques for advanced battery management systems - Part I: SOC estimation, in: Proceedings of American Control Conference, 2012, pp. 559–565.

[16] O. Barbarisi, F. Vasca, L. Glielmo, State of charge Kalman filter estimator for automotive batteries, Control Engineering Practice 14 (3) (2006) 267–275.

[17] M. McIntyre, T. Burg, D. Dawson, B. Xian, Adaptive state of charge (SOC) estimator for a battery, in: Proceedings of American Control Conference, 2006, pp. 5740–5744.

[18] S. Santhanagopalan, Q. Guo, P. Ramadass, R. E. White, Review of models for predicting the cycling performance of lithium ion batteries, Journal of Power Sources 156 (2) (2006) 620–628.

[19] M. Guo, G. Sikha, R. E. White, Single-particle model for a lithium-ion cell: Thermal behavior, Journal of The Electrochemical Society 158 (2) (2011) A122–A132.

[20] M. Coleman, C. K. Lee, C. Zhu, W. G. Hurley, State-of-Charge determination from EMF voltage estimation: Using impedance, terminal voltage, and current for lead-acid and lithium-ion batteries, IEEE Transactions on Industrial Electronics 54 (5) (2007) 2550–2557.

[21] G. A. F. Seber, C. J. Wild, Nonlinear Regression, Wiley, 2003.

[22] J. F. Van Doren, S. G. Douma, P. M. Van den Hof, J. D. Jansen, O. Bosgra, Identifiability: From qualitative analysis to model structure approximation, in: Proceedings of 15th IFAC Symposium on System Identification, 2009, pp. 664–669.

[23] L. Ljung, Asymptotic behavior of the extended Kalman filter as a parameter estimator for linear systems, IEEE Transactions on Automatic Control 24 (1) (1979) 36–50.

[24] B. Bell, The iterated Kalman filter update as a Gauss-Newton method, IEEE Transactions on Automatic Control 38 (2) (1993) 294–297.

[25] A. Zia, An EM algorithm for nonlinear state estimation with model uncertainties, IEEE Transactions on Signal Processing 56 (3) (2008) 921–936.

[26] J. V. Candy, Bayesian Signal Processing: Classical, Modern and Particle Filtering Methods, Wiley, 2009.

[27] L. Ljung (Ed.), System Identification: Theory for the User, 2nd Edition, Prentice Hall PTR, Upper Saddle River, NJ, USA, 1999.